Journal of Thermal Analysis and Calorimetry
https://doi.org/10.1007/s10973-024-13018-6

Microstructural Examination and Thermodynamic Analysis of Sn-1.5Ag-0.5Cu-x mass% Ni Lead-Free Solder Alloys

E. A. Eid[1] · A. Fawzy[2] · M. M. Mansour[2] · G. Saad[2] · M. Amin[3]

Received: 24 August 2023 / Accepted: 25 February 2024

Abstract

The diminutive additions of nickel (Ni) element have been fused to Sn-1.5Ag-0.5 mass% Cu (SAC155) lead-free solder alloy. The study was examined experimentally and computationally (using JMatPro software program) the microstructural features, thermal behavior, density, thermal diffusivity, and conductivity as well as tensile stress strain of the Sn-1.5Ag-0.5Cu-x mass %Ni (x = 0.00, 0.05, 0.10, 0.20, and 0.50) solder alloys (SAC155-xNi). The fusing additions of Ni have a little impact on the melting point of SAC155 alloy which increasing from 502 to 504.2K. The microstructure of SAC155 solder alloy included coarse grains of β-Sn besides, large eutectic regions, and embedded IMCs of Ag_3Sn and Cu_6Sn_5. The computed values of Gibbs free energy (G) during solidification of the β-Sn phase, Ag_3Sn, and Sn_3Sn_4 IMCs show the stability at -130.7×10^3J.kg^{-1}, -157.7×10^3J.kg^{-1}, and -377.13×10^3J.kg^{-1}, respectively. The SAC155-xNi alloys involved finer β-Sn grains, large fibrous eutectic regions, $(Cu,Ni)_6Sn_5$ and $(Cu,Ni)_3Sn_4$ IMCs. The G of Cu_6Sn_5 decreased from -233.1×10^3J.kg^{-1} to -317.9×10^3 J.kg^{-1} when Ni content increased up to 0.25 mass %, then stable and steady at -318.4×10^3J.kg^{-1} with more addition of Ni element. The formation of the $(Cu, Ni)_6Sn_5$ and $(Ni, Cu)_3Sn_4$ IMCs is motivated by the lowest Gibbs free energy, especially when Ni mass% is added to a sufficient level. The measured and computed values of specific heat at constant pressure (C_p) of SAC155-xNi alloys show a good matching especially at lower temperatures and a little mismatch at high temperatures which decreases with increasing Ni content. The activation energy of atomic arrangement (Q) increased from 11.36 to 13.41kJ.mole^{-1} with increasing Ni content in SAC155-xNi alloys. Thermal diffusivity (α) and conductivity (κ) of SAC155-xNi gradually decreased with increasing temperature in the range from 303 to 423 K and/or Ni content in alloys. The measured values of (κ) are slightly lower than the computed value at similar temperatures of the SAC155-xNi alloys. The decrease in (κ) may be assigned to scattering the electrons or reducing the phonon contributions due to the presence of various solute atoms and different IMCs. The results of stress-strain graphs reveal the enhancement of YS and UTS for all Ni-containing alloys. The improvement of the yield stress (YS) and ultimate tensile strength (UTS) of Ni-containing alloys is attributed to the uniform distribution of the IMCs, the reduction of β-Sn grain size, and the smoothed enlargement of the eutectic region.

Keywords Pb-free solder · Microstructure · Thermal analysis · DSC · Thermodynamic calculation · Specific heat capacity · Thermal diffusivity Stress-strain

Introduction

The miniaturization of electronic devices has led to a growing interest in the thermal management of solder alloys. Research into the thermal characteristics of solder alloys has become increasingly significant in recent decades, as it plays a crucial role in controlling their properties [1]. The evaluation of heat transfer behaviors is highly attractive in the design of solder systems. Investigation of the thermal behavior, specific heat, thermal diffusivity, and thermal conductivity equations is crucial for comprehending the mechanism

✉ E. A. Eid
dr_eid_hti@yahoo.com; eid.abdelbast@hti.edu.eg

1 Basic Science Department, Higher Technological Institute, 10th of Ramadan City 44629, Egypt

2 Physics Department, Faculty of Education, Ain Shams University, P.O. Box 5101, Heliopolis, Roxy 11771, Cairo, Egypt

3 Mechanical Engineering Department, Higher Technological Institute, 10th of Ramadan City 44629, Egypt

Published online: 03 June 2024

of heat transfer. Sn-Ag-Cu (SAC) alloys are essential and cannot be ignored in the electronic packaging industry. SAC alloys possess remarkable thermal conductivity, thermal stability, and mechanical properties, making them highly attractive in the microelectronic industries [2–4]. Worthy, the incorporation of new soldering connections with microelectronic chips supports the security of electronic industries and increases the productivity of devices in their daily lives [5]. Additionally, usage of Pb-free solder alloys has led to a substantial decrease in hazardous waste produced during manufacturing. Developing sustainable Pb-free solder alloys is a significant challenge. Balancing the health of humanity with the integrity of manufacturing lines is essential to ensure extraordinary quality and reliability [6].

Low silver content solder alloys in SAC, such as SAC 105 and SAC 107, are widely used in electronics assembly. They introduce high mechanical strength, and good electrical and thermal conductivity attributes, making them suitable for high-stress duty [3, 7]. Additionally, they have approximately low melting points and good wetting with copper circuit board surfaces (CBS), making them easier to utilize in soldering procedures. [8, 9]. However, this category of SAC alloys has several disadvantages that restrict their usage in electronic packaging applications. It could form brittle intermetallic compounds (IMCs) over CBS, especially in power circuits at high-thermal stress applications [9]. Also, their melting points are relatively high compared to other lead-free alternatives, e.g., Sn-Zn [6, 10–12]. Therefore, there is a high probability of microcracking in the CBS and/or damage to delicate electronic components during the soldering process at high temperatures [12–14].

Several research articles have improved the physical characteristics of SAC alloys of low silver content via the fusing of nickel (Ni) with their compositions [2–4, 7–9]. Generally, their IMCs named $(Cu, Ni)_6Sn_5$, Ag_3Sn, and Ni3Sn4 are located in eutectic regions and around β-Sn grains [2–4, 7–9, 15, 16]. The size, distribution, and morphology of these IMCs are dependent on the alloy's processing conditions and the concentration of the alloying elements [17]. Unfortunately, little studies have investigated the thermal conductance and the influence of Ni addition to solder alloys [18–20]. R. Oliveira et.al. [19] correlated the results of solidification experiments with mathematical modeling of an interfacial thermal conductance between the Ni and/or Cu substrates and the Sn-0.5mass%Al alloy. They reported that, the IMC of Al-rich phase precipitated at the interfacial reaction layers of Cu and Ni substrates and the dendritic/cellular morphologies predominate in during solidification in Ni substrate higher than that observed for the Sn–Al/Cu couple. The study conducted by L.S. Silva et al. [20] aimed to analyze the phase transitions of $Sn_{99.1-x}Cu_{0.9}Ag_x$ alloys with varying Ag content (x = 0, 1.5, and 3.5). The research was carried out to investigate the changes in thermal behavior of melting and solidification points, as well as the microstructures of these alloys and intermetallic compounds produced while cooling in air after heat treatment on contact with a copper substrate. The results showed that adding Ag to the $Sn_{99.1}Cu_{0.9}$ alloy led to changes in the thermal behavior of their melting and solidification points. Also, the presence of silver induced the formation of the Ag_3Sn phase and decreased the amount of the Cu_6Sn_5 compound. A study by El Daly et al. has shown that adding 0.05% nickel to the Sn-2Ag-0.5Cu solder alloy can improve its mechanical properties. This improvement is related to a decrease in grain boundary sliding and dislocation activity during plastic deformation [3, 21, 22]. It is crucial to note that excessive quantities of nickel could form brittle IMCs, which may compromise the alloy's mechanical and thermal properties [23]. Therefore, careful balancing of the Ni additions to SAC alloys is necessary to obtain the optimization of the alloy's microstructure to ensure its reliable performance as well as decent thermal behavior.

The objective of this study is to develop new low-silver content SAC lead-free solder alloys for use in electronic packaging. The new solder alloy should possess excellent physical and mechanical properties, including good thermal behavior and conductance. Therefore, the research strategy depends on two approaches; firstly, JMatPro software simulation used to reach the optimization composition of low silver content of Sn–Ag–Cu. The Sn-1.5Ag-0.5Cu composition is optimum low silver content solder alloy which is consider the based matrix that reinforced via alloying an element. Secondly, different minor additions of Ni element have been fused with Sn-1.5Ag-0.5 mass %Cu to reach a careful balancing of IMCs and the alloy's microstructure to achieve its reliable performance as well as decent thermal behavior. Moreover, the study was examined experimentally the microstructural features, thermal behavior, density, thermal diffusivity, and conductivity as well as tensile stress strain of the Sn-1.5Ag-0.5Cu-x mass %Ni (x = 0.00, 0.05, 0.10, 0.20, and 0.50) solder alloys (SAC155-xNi). Furthermore, the JMatPro simulation outcomes of thermal parameters (i.e., specific heat, density, thermal diffusivity, and thermal conductivity) compared with experimental findings for all tested alloys.

Experimental Procedure

Alloys Preparation

High-purity Sn, Ag, Cu, and Ni (99.99%) were used as raw materials to prepare the studied alloys. The raw materials were melted in an electric furnace at 923 K for 2 h to ensure complete dissolution of ingredient compositions. Then, ingots were cast into a steel mold to form rod-like specimens with a diameter of about 15 mm in air. The alloys were remelted and recast three times to achieve a homogeneous alloying and then were solidified in a steel mold to obtain a chill cast ingot with cooling rate of 20K.min^{-1}. This cooling rate was used to create a uniform microstructure and simulate those used in microelectronic packages [12]. X-ray fluorescence (XRF) was originally used to determine the elemental composition of the alloys being studied. Table 1 presents the desired elemental composition of the investigated alloy, which was confirmed by the XRF graphs of the (SAC155-X Ni).

Microstructure Analysis

Part of the prepared solder rods was sliced into $1.5, 0.2, 0.2 cm^3$ tested specimens using an electro-discharge wire cut machine. Afterward, they were homogenized at $393K$ for 2 h to remove interior mechanical residual stresses and attain stable microstructure. The alloys' samples were encased in epoxy; then, their surface was meticulously ground and polished to perfection using metallographic techniques. The samples' scratch-free surfaces were achieved using an even finer abrasive. The samples were then subjected to an etching process, which involved using a precise solution containing 2.0% HNO_3, 3.0% HCl, and 95.0% ethyl alcohol (by volume) at room temperature for a duration of 15 s. Following this, the samples were carefully transferred to water and meticulously dried using filtering paper. The morphological features of alloys were examined using optical and scanning electron microscopy linked with energy-dispersive X-ray spectrometry (EDXS) unit. The morphological features of alloys were studied utilizing ImageJ software to evaluate the size of different phases of prepared alloys. The crystalline phases in the alloys were pronounced by X-ray diffractometry (XRD) using CuK-α radiation at $20 \times 10^{-3} A$ and $40 \times 10^{3} V$. The scanning speed was 1.0°/min, and the diffraction angles (2θ) ranged from 20° to 80°.

Differential Scanning Calorimetry Measurements

The thermal behavior of the studied alloys was measured using thermal analyzer Shimadzu DSC-60 for determination of phase transition temperatures and related heat effects. The DSC instrument was calibrated using the melting points and the heat of melting of pure Ag and Cu. The samples were placed in alumina (Al_2O_3) pans, and DSC heating curves were recorded under a protective flowing Argon atmosphere with a heating rate of 5 K.min^{-1}. The samples weighed on average about 50 mg, and an empty alumina pan was used as a reference material. The specific heat C_p of the SAC155-xNi alloys was measured through the heat flux method. The studied alloys were sliced into 1.0 mm thickness to get good thermal contact with the crucible. Samples were heated from 303 to 573 K with a heating rate of 5 K.min^{-1}. Accordingly, the specific heat can be obtained by Eq. (1) [24]:

$$C_{p,\,sam} = \frac{m_{al}}{m_{sam}} \frac{\Delta H_{sam}}{\Delta H_{al}} C_{p,al} \tag{1}$$

where subscripts 'sam' and 'al' refer to the sample and alumina, respectively, m (kg) the mass, ΔH the heat flow. Furthermore, we can determine the latent heat of fusion (ΔH) of SAC155-x Ni alloys using Eq. (2) [6].

$$\Delta H = k\frac{A}{m} \tag{2}$$

k is the calibration coefficient based on crucible shape, m is sample mass, and A is the endothermic peak area.

Density Measurements

The density (ρ) of SAC155-x Ni alloys is obtained from the Archimedes (buoyancy) method by weighting the sample in the air and in the submersion liquid. Equation 3 is applied, the m_o is the mass of sample in air, m_1 is the mass in paraffin oil of the density $\rho_{liq.} = 850$ kg.m^{-3}.

$$\rho = \frac{m_o}{m_o - m_1} \rho_{liq.} \tag{3}$$

Densities of SAC155-x Ni alloys measured at different temperatures by utilizing kit linked to high accuracy computerized electronic balance.

Table 1 Quantity of mass elements % and XRF elemental compositions in the SAC155- x Ni alloys (mass %)

Name of alloy	Ag		Cu		Ni		Sn
	MASS %	XRF %	MASS %	XRF %	MASS %	XRF %	
SAC155-0.00 Ni	1.5	1.497 ± 0.04	0.5	0.49 ± 0.043	0.0	0.000	Balance
SAC155-0.05 Ni	1.5	1.51 ± 0.043	0.5	0.543 ± 0.041	0.05	0.075 ± 0.028	Balance
SAC155-0.10 Ni	1.5	1.542 ± 0.43	0.5	0.539 ± 0.037	0.1	0.123 ± 0.025	Balance
SAC155-0.20 Ni	1.5	1.512 ± 0.041	0.5	0.52 ± 0.032	0.2	0.216 ± 0.012	Balance
SAC155-0.50 Ni	1.5	1.568 ± 0.042	0.5	0.539 ± 0.038	0.5	0.496 ± 0.021	Balance

Determination of Thermal Diffusivity and Thermal Conductivity

The thermal diffusivity and thermal conductivity of the samples under study were examined using the flash method developed by Parker et al. [25]. In this method, a disk specimen's front face is briefly exposed to an energy pulse generated by a heat source. Simultaneously, the temperature of the rear face is continuously recorded as a function of time. The thermal diffusivity is then calculated using Eq. (4) [26, 27]:

$$\alpha = 1.37\frac{L^2}{\pi^2 t_{1/2}} = 0.1388\frac{L^2}{t_{1/2}} \quad (4)$$

where L is the thickness of the sample, $t_{1/2}$ is the half-rise time, which represents the time required for the rear-face temperature to reach the half of the maximal temperature increase. In the current study, TA Instruments Discovery Xenon Flash (DXF-500) instrument was used for measurement of thermal diffusivity at several points over the temperature range 303–423 K. The prepared alloy samples were shaped into 2-mm-thick round disks with 12.5 mm diameter and plane-parallel ground end faces. The samples were placed in a vacuum furnace and heated to a measurement temperature. When the furnace had reached the required temperature, the front face of the specimen was irradiated by a very short energy pulse from the xenon lamp. Temperature of the rear face of the sample was recorded via the nitrogen-cooled IR temperature detector (In Sb sensor) with very fast thermal response and the high-speed data acquisition system. Additionally, the thermal conductivity $\kappa\left(\mathrm{W}\cdot\mathrm{m}^{-1}\cdot\mathrm{K}^{-1}\right)$ of a sample is calculated from Eq. (5):

$$\kappa = \alpha \cdot \rho \cdot C_{\mathrm{p}} \quad (5)$$

where $\alpha\left(\mathrm{m}^2.\mathrm{s}^{-1}\right)$ is the thermal diffusivity, $C_{\mathrm{p}}\left(\mathrm{J.kg}^{-1}.\mathrm{K}^{-1}\right)$ the specific heat, and $\rho\left(\mathrm{kg.\ m}^{-3}\right)$ the bulk density.

Stress–Strain Tensile Measurements.

To perform stress–strain tensile tests, the bars of ingots were cold drawn into wires with a radius of 1.5 mm through mechanical dragging. All tested specimens were heated to a temperature of 413 K for 120 min to eliminate any cold working defects and achieve a stable microstructure. The tensile tests conducted using an automated universal tensile machine that was equipped with an electric heater. The specimens of length 90 mm underwent testing at a temperature of 303 K under strain rate $7.82 \times 10^{-4}\mathrm{s}^{-1}$. It is worth noting that each point in tensile data is representative of the mean values of four tests.

Results and Discussion

Microstructures of SAC155-x Ni Alloys

Figure 1(a-e) exhibits the SEM images of the studied alloys. Also, Table 2 lists the average compositions for the coexisting phases of the tested alloys, which were determined through EDX analysis of the samples. Also, it describes the morphological features of different phases of the SAC155-x Ni alloys.

Figure 1a shows the microstructure of SAC155-0.0Ni solder alloy which included β-Sn as the coarsen bright phase of an average size 118 µm besides large eutectic regions as the dark gray phase. Furthermore, Ag_3Sn IMC embedded in eutectic area as the micro-needles of an average length 26.5 µm. The Cu_6Sn_5 IMC emerges as the small murky gray platelets of an average area 50.8 µm^2 scattered around the boundary of the β-Sn phase or coexist within eutectic regions. Cu_6Sn_5 IMC is a hexagonal unit cell intermetallic compound that forms when Cu and Sn react that depending on the temperature and composition [15, 16]. The 0.05 Ni addition manifests a gray network-like eutectic region as well as a great change in the shape and size of IMC and modified their distribution as shown in Fig. 1b. Furthermore, the SAC155-(0.2, 0.5) %Ni microstructure was composed of the fine β-Sn grains of an average size 68.2 and 13.86 µm, respectively, and large eutectic region which containing mixed needles of Ag_3Sn, and polygon sticks of $(Cu,Ni)_6Sn_5$ IMC (dark gray phase), as shown in Fig. 1c-d. Generally, the Ni containing alloys have modified rods-like Cu_6Sn_5 to $(Cu,Ni)_6Sn_5$ IMC that formed by replaced Cu atoms by Ni atoms during crystallization process [28].

Furthermore, great changes were observed in the alloy's phases shape as well as materialization of new phases of polygon-like shape of $(Ni, Cu)_3Sn_4$ and big hexagonal-like shape of $Cu_8Ni_3Sn_9$ of an average area 105.2, 3479.7 µm, respectively, after adding 0.5 mass % Ni, as exhibited in Fig. 1e. The EDX analysis of the precipitates $(Ni, Cu)_3Sn_4$ in SAC155-0.5Ni alloy was confirmed and is listed in Table 2. Also, the eutectic regions transformed to fiber-like with long thin needles of Ag_3Sn and fine dot-shaped precipitates at the surface of β-Sn grains (Seen Fig. 1e). The $(Cu, Ni)_6Sn_5$ intermetallic compound exhibits a preference for the formation of discontinuous grains at their interfaces. The grains eventually transform into a lamellar microstructure. Afterward, dendrites begin to transform from the lamellar microstructure into the fibrous structure. The EDXS analyzer was used to identify the qualitative elemental composition of the intermetallic compounds (IMCs) and the observed phases of the SAC155-X Ni alloys. Figure 2a-d displays the EDXS analysis of SAC155-0.5Ni alloy; the large eutectic areas were found to contain Sn, Ag, Cu, and Ni.

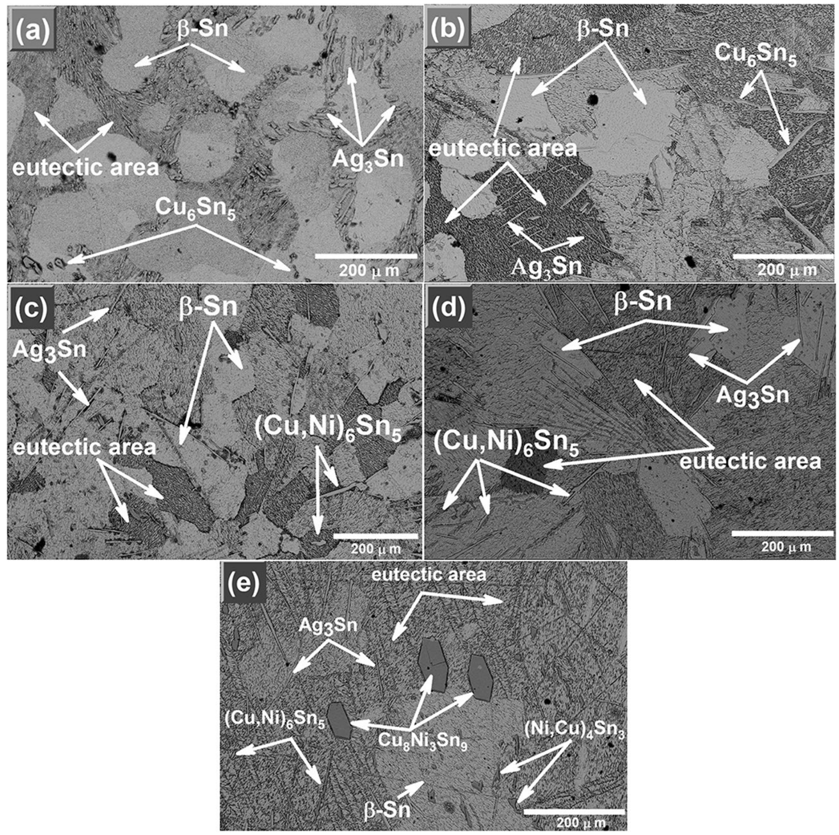

Fig. 1 **a**-**e** SEM micrographs of **a** SAC155-0.0 Ni, **b** SAC155-0.05 Ni, **c** SAC155-0.1Ni, **d** SAC155-0.2 Ni, and **e** SAC155-0.5 Ni solders alloys

Table 2 lists the average compositions for the coexisting phases of the tested alloys, which were determined through EDXS analysis of the samples. Additionally, EDX elemental mapping is a technique that uses X-rays to identify the elements in a sample and show their distribution in a two-dimensional image. It is useful for studying the elemental composition and their distribution. It was implemented to analyze the elemental distribution in the SAC155-0.5Ni alloy, as shown in Fig. 3. It seems that the elements are distributed almost uniformly within the β-Sn phase. It is evident that the SAC155-0.5 Ni alloy contains Ag_3Sn, $(Ni, Cu)_6Sn_5$, $(Cu, Ni)_3Sn_4$, and $Cu_8Ni_3Sn_9$ intermetallic compounds.

Incorporating Ni into the SAC155 alloy not only enhances the formation of $(Cu, Ni)_6$-Sn_5 but also increases the substitution of Cu atoms with Ni atoms in the lattice. This is due to Ni having no solubility in the β-Sn phase, but a significant solubility in the Cu_6Sn_5 phase. As a result, Ni, like Cu, is transferred from the β-Sn phase to the IMC phase during the growth process [21]. Increasing the amount of Ni in the SAC155-0.5Ni alloy can greatly enhance the formation of $(Ni, Cu)_3Sn_4$ and $Cu_8Ni_3Sn_9$ IMCs. The growth of both $(Cu, Ni)_6Sn_5$ and $(Cu, Ni)_3Sn_4$ as primary phases during the eutectic reaction suggests that the presence of IMCs is not influenced by the rate of nucleation. Also, the presence of $(Cu, Ni)_3Sn_4$ rather than Ni_3Sn_4 suggests that it has easier growth kinetics than Ni_3Sn_4 [29]. Therefore, it is essential to consider the influence of nickel on the formation of IMC and the morphologies of the eutectic zones, particularly in terms of how nickel modifies the interfacial energies between β-Sn and the liquid phase and/or other IMCs [3, 30].

On the other hand, some of IMCs (Cu6Sn5 and Cu3Sn4, (Cu, Ni)6Sn5 and (Ni, Cu)3Sn4) are formed at the interface between solder and substrate during soldering or aging processes. These IMCs are detected in Sn-based solder alloys with Ni or Cu substrates [31, 32]. The growth and morphology of these IMCs can affect the microstructure, mechanical properties, and reliability of the solder joints. Generally, $(Cu, Ni)_6Sn_5$ has a higher melting point, lower diffusion coefficient, and better thermal stability than $(Ni, Cu)_3Sn_4$. However, $(Ni, Cu)_3Sn_4$ has a higher hardness, lower electrical resistivity, and better wettability than (Cu, Ni)6Sn5 [31, 32]. The optimal performance of the alloys depends on the balance between these two IMCs, as well as the effects of other microalloying elements such as Ag, Sb, and Ti. [31–33].

XRD examinations were performed to confirm the crystalline phases formation of the SAC155-x Ni solder alloys. Figure 4 displays the presence of β-Sn, Ag_3Sn, and Cu_6Sn_5 phases in all tested alloy. The diffraction patterns of SAC155-x Ni alloys show significant difference between them. The fundamentals crystalline plans of β-Sn phase

Table 2 Outcomes of SEM–EDX analysis of different phases, morphological features of the SAC155-x Ni investigated alloys

Solder alloy	Microstructure phases	Identified phases	Morphology	Size	Average composition/at%			
					Sn	Ag	Cu	Ni
SAC155-0.00 Ni	Ag_3Sn, Cu_6Sn_5 IMCs, eutectic regions, and nonuniform coarsen β-Sn grains	β-Sn	coarse grains (μm)	118	98.79	0.31	0.48	0
		Eutectic region	small, smoothed	–	98.58	0.19	1.23	0
		Ag_3Sn	needles	26.5	31.10	67.9	1.01	0
		Cu_6Sn_5	Platelets ($μm^2$)	50.8	45.34	0.22	54.43	0
SAC155-0.05 Ni	Ag_3Sn, Cu_6Sn_5 IMCs, rough eutectic region, and nearly finer β-Sn grain	β-Sn	coarse grains (μm)	100.2	98.63	0.21	0.6	0.55
		Eutectic region	small, smoothed	–	96.56	1.23	1.74	0.47
		Ag_3Sn	Long needles rods	45.95	50.97	47.8	0.63	0.59
		Cu_6Sn_5	Big rods ($μm^2$)	252.6	47.18	0.27	52.12	0.42
SAC155-0.20 Ni	Ag_3Sn, $(Cu,Ni)_6Sn_5$ IMCs, smooth large eutectic region, and uniform finer β-Sn grain	β-Sn	small grains (μm)	68.2	98.43	0.32	0.58	0.67
		Eutectic region	small, smoothed	–	96.01	1.30	1.68	1.00
		Ag_3Sn	Long fine needles	38.4	35.02	62.9	1.11	0.9
		$(Cu,Ni)_6Sn_5$	Polygons and big rods ($μm^2$)	227.6	44.71	0.17	37.3	17.8
SAC155-0.50 Ni	Ag_3Sn, $(Cu, Ni)_6Sn_5$, $(Ni, Cu)_3Sn_4$, and $Cu_8Ni_3Sn_9$ IMCs, smoother large eutectic region, and uniform finer β-Sn grain	β-Sn	fine grains (μm)	13.86	97.95	0.34	1.03	0.68
		Eutectic region	small, smoothed	–	91.45	4.73	2.34	1.47
		Ag_3Sn	Long needles	42.25	26.18	69.6	2.17	2.02
		$(Cu, Ni)_6Sn_5$	Polygons platelets and rods ($μm^2$)	208.1	44.82	0.23	44.77	10.2
		$(Ni, Cu)_3Sn_4$	Hexagonal shapes	105.1	59.89	0.14	36.76	19.3
		$Cu_8Ni_3Sn_9$	Wide Hexagonal shapes ($μm^2$)	3479.7	43.94	0.19	40.84	15.1

besides some of IMC's peaks clearly appeared. When Ni was added to the SAC155 alloy, it caused the formation of $(Cu, Ni)_6Sn_5$ instead of the Cu_6Sn_5 IMC. Because Ni atoms have high solubility in the Cu_6Sn_5 phase, enabling them to replace Cu atoms in the IMC lattice [34]. The extra additions of Ni % generate the peaks of Ni_3Sn_4 IMC in SAC155-xNi alloys. The solidification and nucleation rate directly influences the intensity of these peaks. The crystalline plane intensities of the different crystal phases in SAC155-xNi alloys exhibit varying values.

In general, the presence of Ni in the SAC155-xNi alloys not only affects the growth kinetics of crystalline IMCs, but also has a significant impact on the interfacial energies at various interfaces [29]. Since, the presence of Ni element may be enhancing the solubility between Ag and Sn in the Sn-Ag-Cu system [35]. Also, the Ni atoms may be playing a crucial role in diminishing the reactivity of Sn at the SAC system [36]. Therefore, reducing the size of the Ag_3Sn IMC is a highly effective way for obtaining an exceptionally desirable material. Thus, the finer Ag_3Sn IMC is distributed throughout the solder, acts as heterogeneous obstacles sites for mobile dislocations and exhibits a better performance. This suggests that the fusion of Ni into SAC155 alloy could potentially enhance the overall performance and reliability of solder joints in electronic applications.

Thermodynamic Simulation

During the solidification process of the SAC system, the main reactions are [17, 37].

$$Sn_{\text{liquid}} \rightarrow \beta - Sn_{\text{solid}}$$

$$Ag + Sn \rightarrow Ag_3Sn$$

$$Sn_{\text{liquid}} \rightarrow \beta - Sn_{\text{solid}}$$

During the solidification process of the SAC-Ni system, the main reactions are [37].

$$Sn_{\text{liquid}} \rightarrow \beta - Sn_{\text{solid}}$$

$$\mathrm{Cu + Sn \rightarrow Cu_6Sn_5}$$

$$\mathrm{Cu + Sn + Ni \rightarrow (Cu,\ Ni)_6Sn_5}$$

$$\mathrm{Ni + Sn \rightarrow Ni_3Sn_4}$$

$$\mathrm{Ni + Cu + Sn+ \rightarrow (Ni,\ Cu)_3Sn_4}$$

The Ni content is the primary influence on these reactions. When the Ni percentage reaches a specific level, it results in the reaction between Cu and Ni with Sn. Firstly, the formation of Cu_6Sn_5 IMC occurs, while Ni dissolves

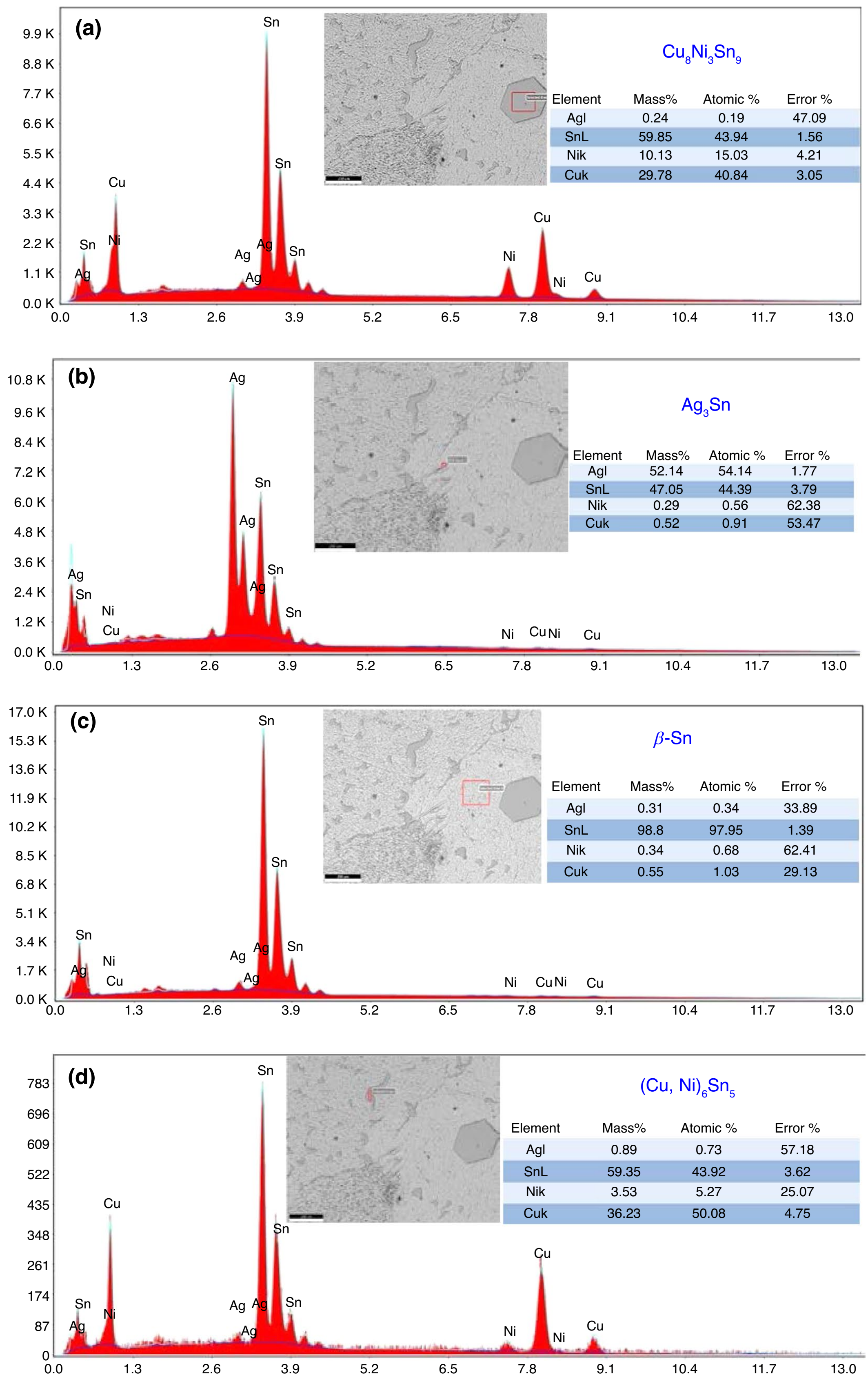

Fig. 2 **a-d** EDXS Analysis of different phases in SAC155-0.5 Ni solders alloys

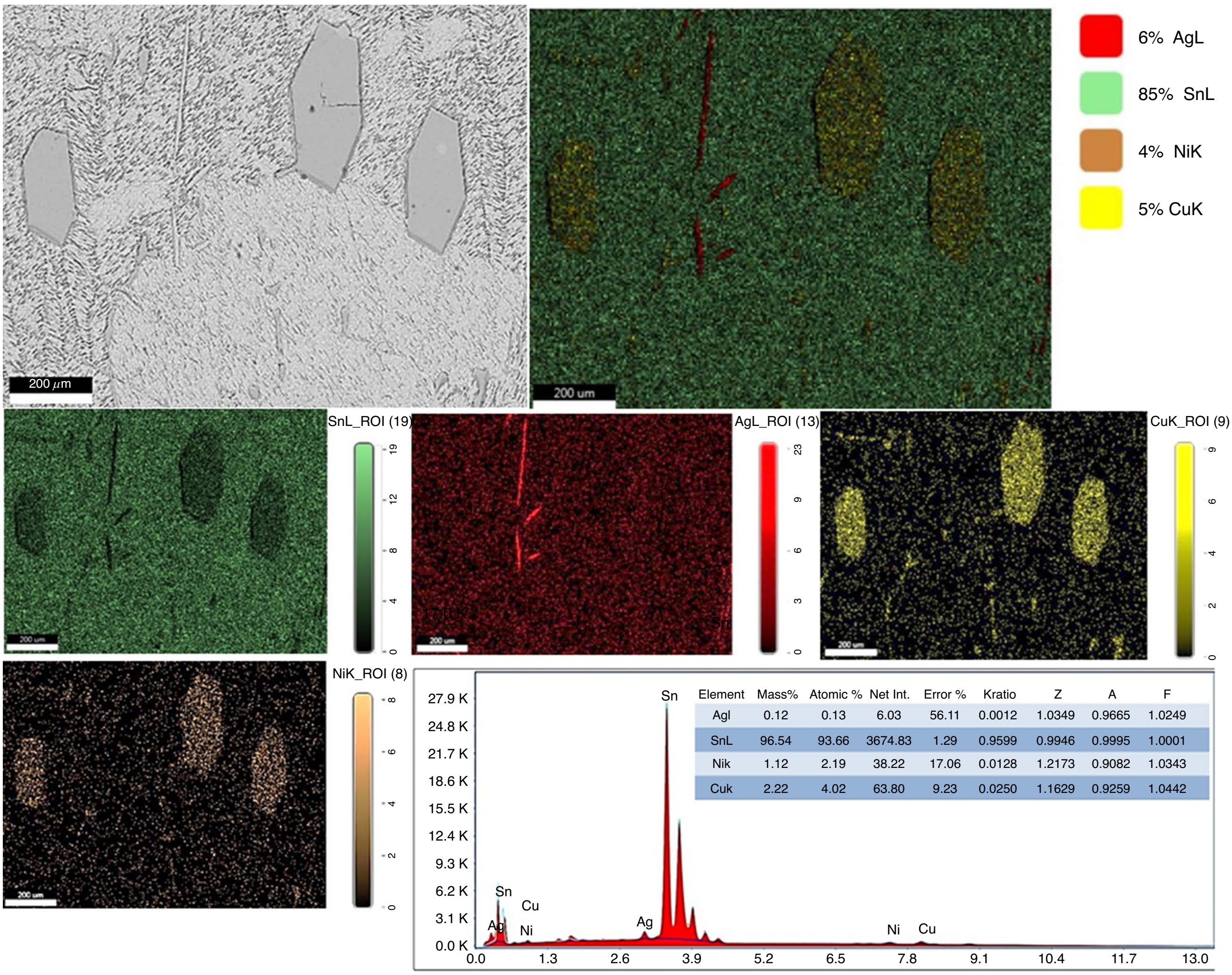

Fig. 3 Backscattered electron compositional images of distribution of SAC155-0.5 Ni solders alloys

in (Cu, Ni)$_6$Sn$_5$. The embryonic reaction between nickel and tin is the generation of Ni_3Sn_4, especially when more Ni is added. Furthermore, the Cu element undergoes a reaction with Ni, resulting in the formation of a symbiotic solid solution known as (Ni, Cu)$_3$Sn$_4$ IMC [37]. Hence, the incorporation of Ni plays a central role in influencing the reaction of solidification.

The tendency of a reaction's mixing is dictated by the thermodynamic relationship between elements. Equation (6) provides the relationship between Gibbs free energy G, enthalpy, and entropy of mixing [37, 38].

$$\Delta G = \Delta H - T\Delta S \tag{6}$$

In thermodynamic chemistry, the Gibbs free energy (***G***) of a system is used as a criterion for determining the priority of a reaction. It can be expressed by Eq. (7), where ***H*** is enthalpy, *T* is temperature, and ***S*** is entropy [37].

$$G = G^{\mathrm{I}} + G^{\mathrm{E}} \tag{7}$$

The ideal molar-free energy, G^{I}, and the excessive molar-free energy, G^{E}, are both important in this study. Equation (8) provides a concise representation for deriving the value of G^{I}, whereas Eq. (6–9) ingeniously employs the powerful JMatPro software to accurately compute G^{E} [37, 38].

$$G^{\mathrm{I}} = G^0 + \Delta G^{\mathrm{I}} = \sum_{\mathrm{i}} X_{\mathrm{i}} G_{\mathrm{i}}^0 + RT \sum_{\mathrm{i}} X_{\mathrm{i}} \ln X_{\mathrm{i}} \tag{8}$$

$$G^{\mathrm{E}} = \sum_{\mathrm{i}} \sum_{\mathrm{i}} X_{\mathrm{i}} X_{\mathrm{j}} \sum_{\mathrm{v}} \Omega_{\mathrm{v}} \left(X_{\mathrm{i}} - X_{\mathrm{j}}\right)^{\mathrm{v}} \tag{9}$$

At a given temperature ***T***, the molar free energy of composition-i ($\boldsymbol{G}_{\mathrm{i}}^0$) can be expressed as a function of the molar

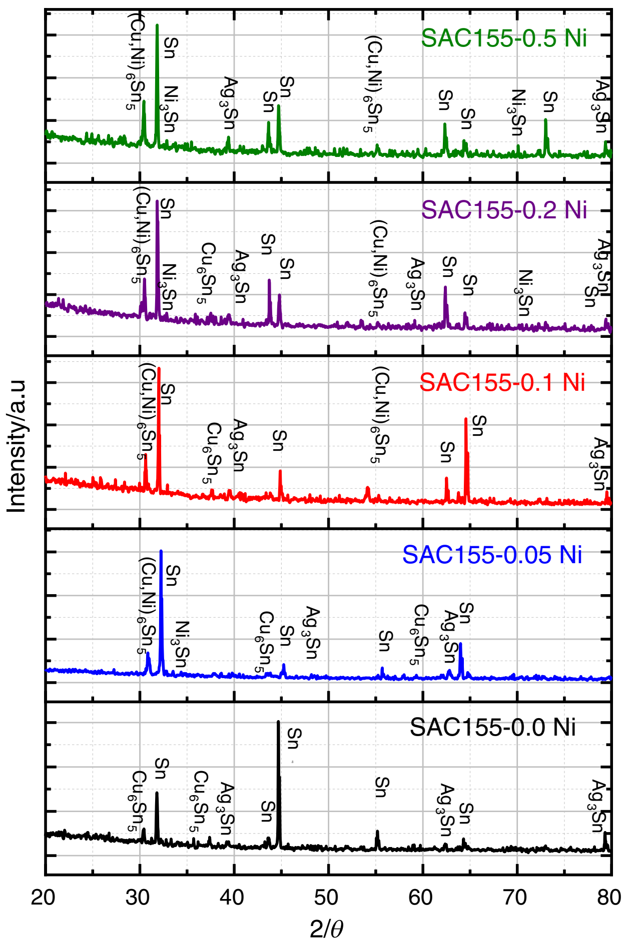

Fig. 4 XRD Patterns for the SAC155-x Ni solder alloys

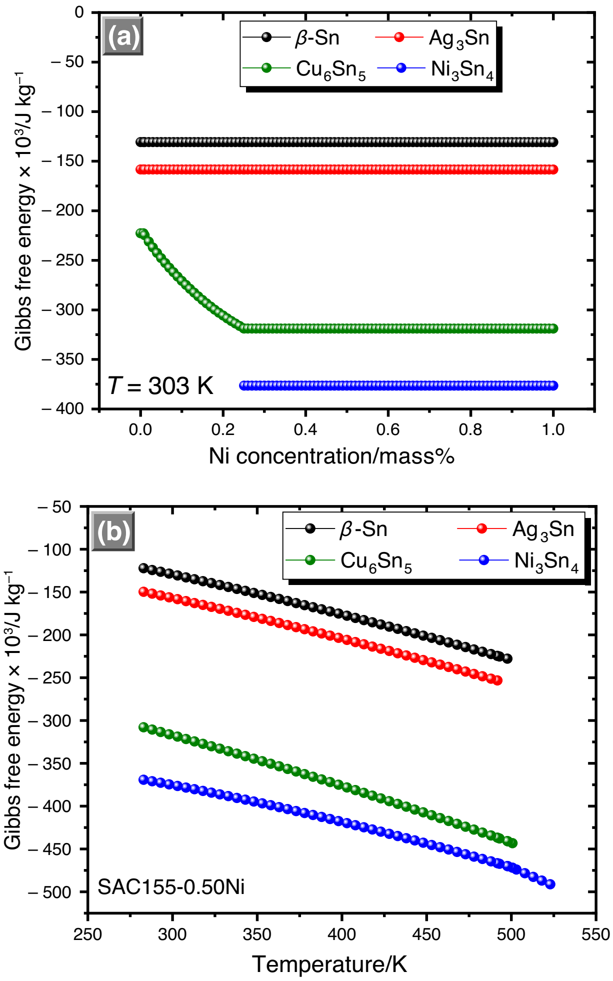

Fig. 5 (**a-b**) Gibbs free energy of different phases in SAC155-xNi alloys as function in (**a**) Ni concentration mass% (**b**) Temperature (K)

fraction of composition-i ($\boldsymbol{X}_{\mathrm{i}}$) and the gas constant ($\boldsymbol{R}$). In addition, the interaction parameter ($\boldsymbol{\Omega}_{\mathrm{v}}$) can be defined as a function of $\boldsymbol{X}_{\mathrm{i}}$.

According to the above equations, Fig. 5a displays the Gibbs free energy of the distinct phases that formed after the solidification of the SAC155-xNi alloys as a function of Ni concentration, calculated using JMatPro at a temperature of 303 K. With variation of Ni content up to 1.0 wt.% into the base SAC155 alloy, it is indicated that all elemental fraction of the β-Sn phase, Ag_3Sn and Sn_3Sn_4 IMCs has the Gibbs free energies that stable at $-130.7 \times 10^3 J.kg^{-1}$, $-157.7 \times 10^3 J.kg^{-1}$, and $-377.13 \times 10^3 J.kg^{-1}$, respectively. Additionally, the Gibbs free energies of Cu_6Sn_5 decreased from $-233.1 \times 10^3 J.kg^{-1}$ to $-317.9 \times 10^3 J.kg^{-1}$ when Ni content increased up to 0.25 mass%, then stable and steady at $-318.4 \times 10^3 J\ kg^{-1}$ with more addition of Ni element. This decrease in Gibbs free energy may be related to the ability of Ni atoms to substitute Cu atoms in the lattice of Cu_6Sn_5 IMC. As a result of this modification, $(Cu, Ni)_6Sn_5$ is formed, which helps to achieve solidification equilibrium. It is well-known that the formation of Ni3Sn4 and/or $(Ni, Cu)_3Sn_4$ IMCs is motivated by the lowest Gibbs free energy, especially when Ni mass% is added to a sufficient level. As a result, it is possible for tiny amounts of Ni to diffuse into the Cu-Sn IMC due to the influence of Gibbs's free energy.

JMatPro software has been employed to perform thermodynamic calculations and determine the solidification process of SAC155-xNi alloys [39]. During equilibrium, the Ag_3Sn, Cu_6Sn_5 IMCs, and β-Sn phases begin to solidify. Different temperatures were used to calculate the solid fraction of separate phases in SAC155-xNi alloys. Figure 6a-b displayed the temperature-dependent and solid volume fraction (mass%) of phases from 673 K400 to 298 K for SAC155-0.0 Ni and SAC155-0.5 Ni alloys. Also, the results of these calculations are documented in Table 3. Using thermodynamic calculations, it predicted the formation of Ni_3Sn_4 IMC by incorporating 0.5 mass% of nickel into the SAC155 alloy. The accuracy of the

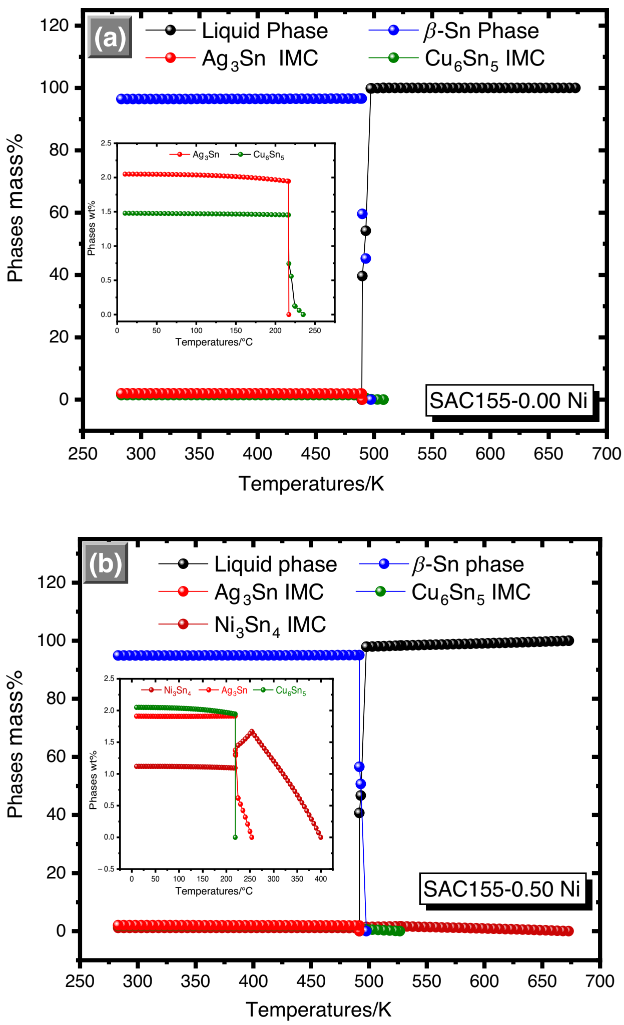

Fig. 6 (**a**-**b**) Relationship between phases fraction mass% and temperature into solder alloys **a** SAC155-0.0Ni and **b** SAC155-0.5Ni

results has been validated by examining the microstructure, as shown in Figs. 1–4.

Figure 6a displays that the SAC155.0.0 Ni is near-eutectic composition, so that liquid phase is the first phase to form, and the remaining liquid then solidifies by a simple eutectic-type reaction to β-Sn phase, Ag_3Sn, and Cu_6Sn_5 IMCs. During cooling from 523 to 298 K, the fractions of Cu_6Sn_5 IMCs initially formed and slightly increase tell saturated at 1.48 mass% under cooling. Meanwhile Ag_3Sn IMC formed and saturated at 1.88 to 2.1 mass % during cooling to room temperature.

It should be stressed that the model predicts phases that will be present under equilibrium conditions and therefore predicts multi-constituent phases, rather than normally be found in reality. However, it would be possible to continue the calculations for Ni-containing alloys at the same cooling range. The addition of a Ni content up to 1.0 mass % to the base SAC155 alloy has a profound effect on the formation of the Cu_6Sn_5 IMC, and it is now described as a $(Cu, Ni)_6Sn_5$ IMC (shown in Fig. 7a-b). This is because Ni being the predominant substantial element with Cu crystals. A further increase in Ni level to 0.25% results in the primary Ni_3Sn_4 and or $(Ni, Cu)_3Sn_4$ IMCs, during cooling up to room temperature, as shown in Fig. 7b. Generally, the addition of Ni has great effect on the IMC formation but a little effect on eutectoid reactions or its temperature.

Differential Scanning Calorimetry (DSC) Measurements

Thermal analysis using DSC measurements is a very important tool to investigate the thermal behavior of tested solder alloys. Figure 8a shows the data of enthalpy variation during the melting process of SAC155-xNi solder alloys, and the main findings record in Table 4. Only one endothermal peak exists in each DSC curve during the heating process. The common features of endothermic peaks are started at solidus temperature $\left(T_{sol}\right)$, at which the solid phase starts to transform into liquid phase. These peaks are ended at liquidus temperature $\left(T_{liq.}\right)$ at which solid phase completely changed to liquid phase. The T_{sol} increments from 488.6 to 497.6 K with an increase in the Ni content. The melting temperature (T_{melt}) of Ni-free solder alloy exists at 499.2 K. Meanwhile, the T_{melt} of Ni-containing solder alloys (SAC155-x Ni) raised from 502 to 504.2 K which can be attributed to the high melting temperature of Ni element (1728K) and its low solubility in $\beta - Sn$ phase.

The pasty range or (mushy zone) is the temperature range in which a solder is in a semi-solid state, neither fully solid nor fully liquid. It is calculated by subtracting the solidus temperature from the liquidus temperature of the solder. The pasty range is one of very essential parameters for the soldering process because it estimates the time required for finishing it. The pasty range of SAC155-0.0 Ni, SAC155-0.05 Ni, SAC155-0.1 Ni, SAC155-0.2 Ni and SAC155-0.5 Ni solders, respectively, was 15.0, 9.0, 9.6, 9.6, and 12.1 K which is around to the pasty range for eutectic Sn-Pb solder (11.5 K) [40]. The SAC155-xNi alloys that have a narrow thermal pasty range are favored. This is helpful to avoid the formation of large thermal stress, better wetting, and prevent the production of fillet lifting phenomena [13]. Furthermore, the latent heat values for SAC-x Ni alloys (where $x = 0.0$, 0.05, 0.1, 0.2, and 0.5 mass%) were computed using thermo-graphs in Fig. 8a and are recorded in Table 4. The SAC155-0.5 Ni alloy stands out with its low heat fusion of 44.515×10^3 J.kg^{-1}, making it the most advantageous choice for saving energy compared to other solder compositions.

Table 3 Thermodynamic calculation of different phases % of SAC155- xNi alloys at different temperatures

Alloys	Ni mass %	Temperature Phases %	303 K	343 K	398 K	448 K	498 K
SAC155-0.0 Ni	0	Liquid	0	0	0	0	100
		β-Sn	96.66	96.66	96.68	96.72	0
		Ag_3Sn	2.05	2.04	2.03	1.99	0
		Cu_6Sn_5	1.3	1.3	1.29	1.28	0
SAC155-0.05 Ni	0.05	Liquid	0	0	0	0	99.88
		β-Sn	96.48	96.49	96.51	96.55	0
		Ag_3Sn	2.05	2.04	2.03	1.99	0
		Cu_6Sn_5	1.48	1.47	1.47	1.46	0.12
SAC155-0.1 Ni	0.1	Liquid	0	0	0	0	99.6
		β-Sn	96.32	96.32	96.35	96.39	0
		Ag_3Sn	2.05	2.04	2.02	1.99	0
		Cu_6Sn_5	1.64	1.63	1.63	1.62	0.4
SAC155-0.2 Ni	0.2	Liquid	0	0	0	0	99.16
		β-Sn	96.04	96.04	96.06	96.1	0
		Ag_3Sn	2.04	2.04	2.02	1.99	0
		Cu_6Sn_5	1.92	1.92	1.92	1.91	0.84
SAC155-0.5 Ni	0.5	Liquid	0	0	0	0	97.94
		β-Sn	94.94	94.95	94.97	95.01	0
		Ag_3Sn	2.04	2.03	2.02	1.98	0
		Cu_6Sn_5	1.9	1.9	1.9	1.9	0.6
		Ni_3Sn_4	1.12	1.12	1.12	1.11	1.46

Specific Heat Capacity (C_p)

The specific heat under constant pressure (C_p) obtained from the DSC curves by using Eq. (1). Figure 8b exhibits the measured and computed values of C_p during the melting process of SAC155-xNi solder alloys. The specific heat slightly rises as the temperature increases and reaches the maximum peak at their melting temperature for all studied alloys. However, the specific heat of SAC155-x Ni is nearly independent of Ni content, especially at a temperature range of 323-473 K. This indicates that the addition of a small amount of Ni to Sn-1.5Ag-0.5Cu alloy causes very slight lowering in its specific heat. Furthermore, the specific heat values at constant pressure for SAC155-xNi alloys computed by JMatPro software show, a good match, especially at lower temperatures. However, there is a mismatch at high temperatures that decreases with increasing Ni content.

Moreover, Fig. 9 shows the measured values of maximum specific heat at constant pressure $\left(C_p^{max}\right)$ dependence on Ni content in the tested alloys. Generally, the increment of Ni content in the tested alloys led to lower the values of C_p^{max} from 5.54×10^3 to 4.97×10^3 J.kg^{-1}.K^{-1}. It is indicated that $\boldsymbol{C}_p^{max}$ is important factor for solder material as intrinsic property. The highest $\boldsymbol{C}_\mathbf{p}^{\mathbf{max}}$ was for free Ni-content alloy, suddenly the $\boldsymbol{C}_p^{max}$ value decreased to 5.29×10^3 J.kg^{-1}.K^{-1} at 0.05 mass % Ni which may be due to increasing the molar fraction of IMCs. After that continuous slightly decreased until addition of 0.5 mass % Ni. For a constant mass of all tested alloys and using this equation $\left(Q = m\, \boldsymbol{C}_p^{max} \Delta T\right)$, it is clear that low $\boldsymbol{C}_p^{max}$ value means low energy needed for temperature changing and vice versa. Consequently, the free Ni-content alloy needed maximum thermal energy, meanwhile, SAC155-0.5 Ni alloy required minimum thermal energy to attain the same temperature changing.

The change of specific heat ΔC_p with increasing temperature (T) obeys the experimental low [41].

$$\Delta C_p = Z\left(\frac{N\, Q^2}{R\, T^2}\right) \exp -(Q/R\, T) \tag{10}$$

where $\boldsymbol{N}$ is the number of atoms displaced from the equilibrium position, $\boldsymbol{Q}$ is thermal activation energy of ordering transition, $\boldsymbol{R}$ is the universal gas constant and $\boldsymbol{Z}$ is the coordination number. Regardless of the value of the pre-exponential term, the relation between $\ln\left(\Delta C_p T^2\right)$ and $1000/T$ for all tested solder alloys given straight lines as displayed in Fig. 10. The activation energy of atomic arrangement has been evaluated from the slopes of these lines. Generally, the Q values depend on the Ni content in investigated solder alloys as represented in Fig. 11. The Ni-free alloy has a low energy ordering value of 11.36 kJ.mole^{-1}. Furthermore, the inclusion of Ni in amounts of up to 0.1 mass % is being considered to increase the Q value to 12.57 kJ.mole^{-1}. suddenly

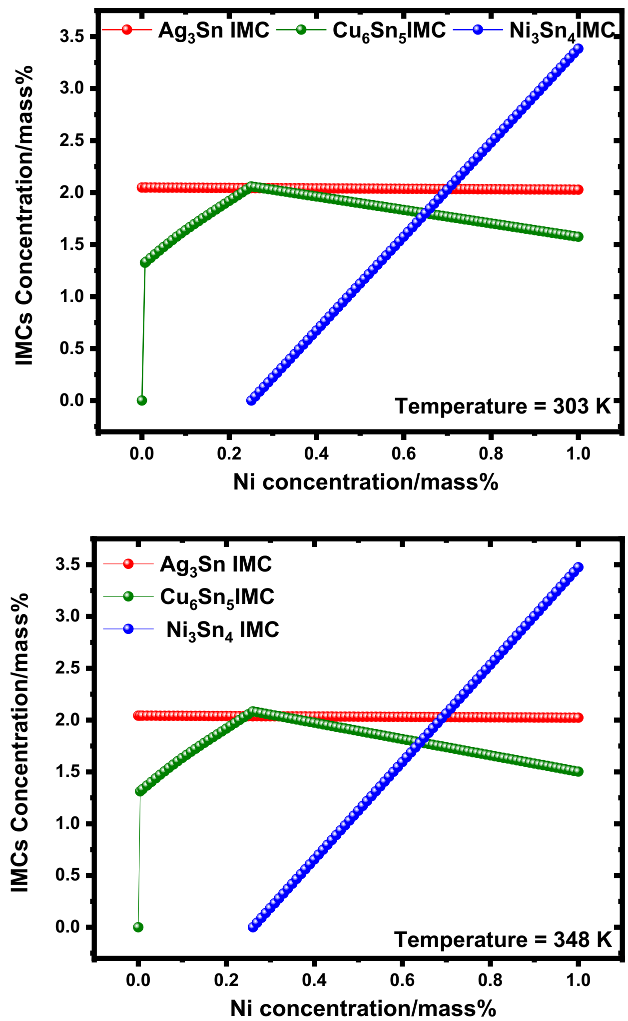

Fig. 7 **a-b** Relationship between IMCs concentrations and Ni mass% into SAC155-xNi alloy at temperature: **a** $T = 303K$ and **b** $T = 348K$

decreases to 11.9 kJ.mole^{-1} at 0.2 mass % Ni and gradually increases again up to 0.5 mass % Ni $\left(13.41\,\text{kJ.mole}^{-1}.\right)$. The fluctuation behavior of the Q values with the different nickel additions can be attributed to the modification processes in microstructural features, which include more formation of additional IMCs with diverse shapes, and homogeneous or heterogeneous distribution in Ni-content solder alloys.

Thermal Diffusivity and Thermal Conductivity

Thermal diffusivity (α) is an important property of solder alloys because it determines how quickly heat can be transferred through the alloy. A high thermal diffusivity value implies that heat can be transferred more quickly, i.e., rapid heat dissipation. So, the study of thermal diffusivity is very important to design solder alloys that are employed in electronic packaging applications. Thermal diffusivity is directly proportional with thermal conductivity coefficient (κ) and inversely proportional to the density (ρ) and specific heat $\left(C_P\right)$ [24].

Figure 12 a-b illustrates the computed values of thermal conductivity and density for SAC155-x Ni solder alloys using JMatPro software, within a temperature range of 298 to 473 K. It is revealed that the values of both ρ and κ decrease with rising temperature and depend on the Ni content in the tested solder alloys. Generally, the thermal conductivity of pure metals decreases with increasing temperature, but the thermal conductivity of alloys may increase, decrease, or remain constant with temperature depending on the relative contributions of the electronic and phonon components [24] Fig. 13.

Figure 12b shows the thermal conductivity (κ) of SAC155-x Ni alloys which decreases with increasing temperature. The κ decreases with rising the Ni content in solder alloy from 65.13 to 63.44 Wm^{-1}K^{-1} at temperature of 298 K, with a reduction of 2.6%. Furthermore, the κ values reduced from 59.76 to 58.52 Wm^{-1}K^{-1} for SAC155-0.0 Ni and SAC155-0.5 Ni alloy at temperature 473 K, respectively, with a little reduction of 2.1%. On other hand, the estimated values κ for tested solder alloy are agreement with the reported thermal conductivity of pure Sn, Sn-37Pb, and Sn-3Ag-0.5Cu eutectic alloys at room temperature are 66.6, 50.9, and 58.1 Wm^{-1}K^{-1}, respectively [19]. Additionally, C. Morando et al. [42] confirmed the thermal conductivity of Sn-Ag alloys depends on the Ag content and the presence of Ag_3Sn intermetallic phase. For example, the thermal conductivity of Sn-10 mass % Ag and Sn-20 mass % Ag alloys at room temperature is about 60.6, 59.4 Wm^{-1}K^{-1}, respectively, Fig. 12.

Indeed, thermal diffusivity values (α) depend on several factors, e.g., testing temperature, the composition of solder alloy, and their microstructure. Figure 14 illustrates the correlation between thermal diffusivity and SAC155-XNi alloys across various temperatures ranging from 323 to 437 K. Obviously, the α value of SAC155-x Ni alloys decreases semi-linearly as the temperature increases. The α value of SAC155-0.5 Ni alloy lowers from 27.18×10^{-4} to 12.71×10^{-4} m^2.s^{-1} as the temperature rises from 323 to 423 K, with a reduction of 53.2%. In addition, the Ni-free alloy demonstrates an impressive decrease in α value by 77.73%. This is clearly demonstrated by the values of $12.66 \times 10^{-4}, 6.82 \times 10^{-4}$ m^2.s^{-1} at same temperatures range. These findings demonstrate that solder alloys with

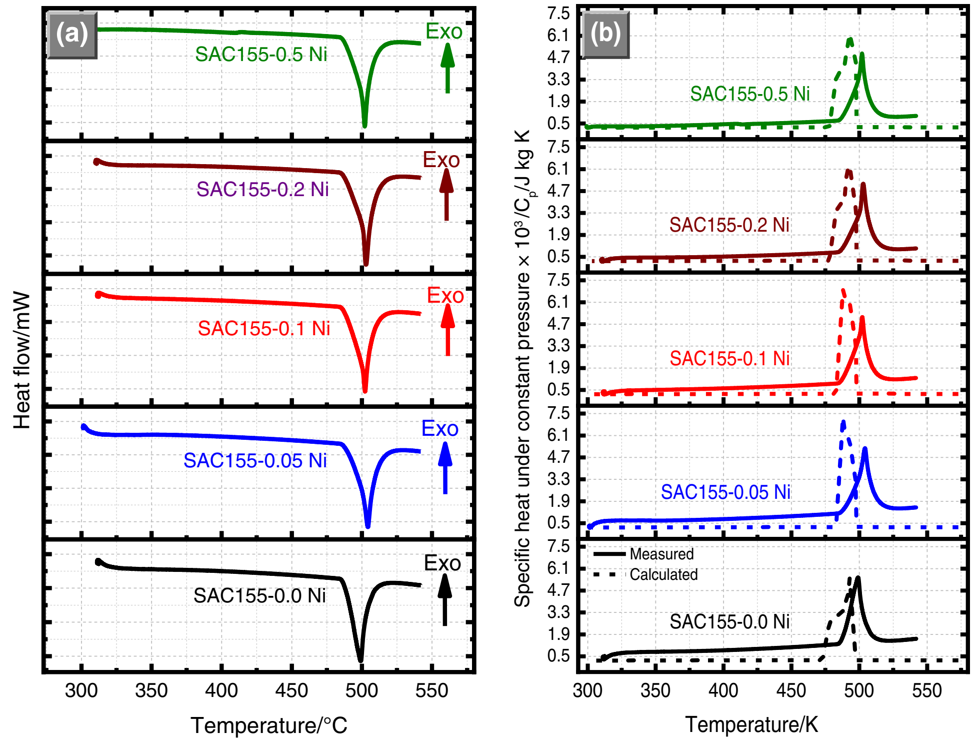

Fig. 8 (**a**-**b**) **a** DSC thermographs during heating, **b** specific heat under constant pressure dependence (measured & calculated) on temperature of SAC155-x Ni lead-free solder alloys

Table 4 The values of solidus ($T_{sol.}$), melting (T_{melt}), liquidus ($T_{liq.}$) temperatures, pasty range, and latent heat of the tested alloys

Alloys	$T_{sol.}$/K	T_{melt}/K	$T_{liq.}$/K	Pasty range/K	Latent heat 10^3/J.kg^{-1}
SAC155-0.00 Ni	488.6	499.2	503.6	15.0	46.98
SAC155-0.05 Ni	497.2	502.0	506.2	9.0	48.09
SAC155-0.10 Ni	498.8	502.1	508.4	9.6	46.48
SAC155-0.20 Ni	497.2	502.2	506.8	9.6	47.97
SAC155-0.50 Ni	497.6	504.2	509.7	12.1	44.515

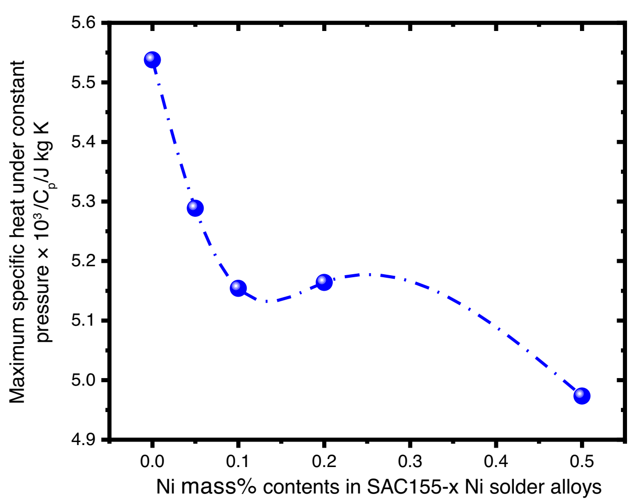

Fig. 9 Maximum specific heat value at constant pressure (C_p^{max}) dependence on Ni concentration in the tested alloys

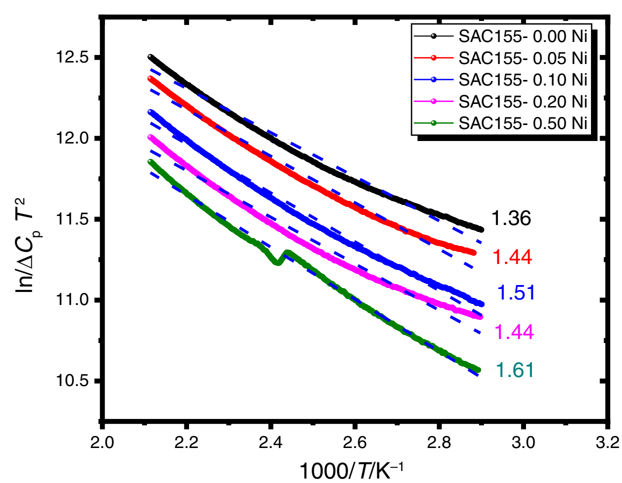

Fig. 10 Dependence relation between ln ($\Delta C_p T^2$) and $1000/T$ for the tested solder

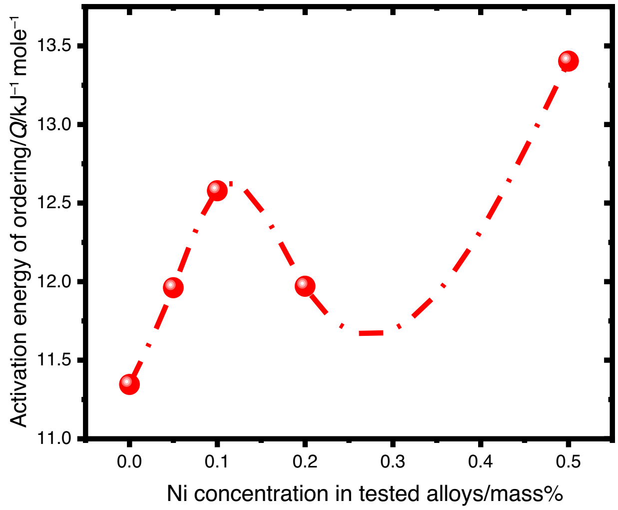

Fig. 11 Activation energy (Q) of ordering transition dependence on Ni concentration in the tested alloys

higher nickel (Ni) content exhibit enhanced heat flow stability during usage, as their thermal diffusivity values exhibit less reduction with rising temperatures. On the other hand, for all tested temperatures, the α value is directly proportional to Ni content in alloys, especially at lower temperatures.

Moreover, thermal conductivity of SAC155-xNi alloys has been investigated experimentally in the temperature range from 303 to 423 K using the flash method. To determine the thermal conductivity coefficient of the studied alloys, we have measured their density, thermal diffusivity, and specific heat capacity values [26, 27]. Table 5 summarized the obtained results of density, specific heat capacity, thermal diffusivity, and thermal conductivity for the SAC155-xNi alloys in the temperature range from 303 to 423 K. Generally, their specific heat capacity slowly increases with increasing temperature, whereas the thermal diffusivity and thermal conductivity gradually decrease. The measured values of thermal conductivity of the SAC155-xNi alloys are close to each other. The thermal conductivities are slightly lower than the computed value for the SAC155-xNi alloys at similar temperatures via JMatPro software. Higher content of Ni alloy did not cause an aggressive decrease of its thermal conductivity. In contrast, thermal conductivity of the SAC155-0.5Ni alloy is somewhat lower than the thermal conductivity of the Ni-free alloy. The reason might be due to the low percentage of Ni element and large fraction of its intermetallic phase in the SAC155-0.5Ni alloy. Generally, the thermal conductivity of an intermetallic phase is lower than the thermal conductivities of the pure constitutive metals. The total thermal conductivity of metals and alloys can be expressed as the sum of electron and phonon (or lattice) contributions. However, in alloys electrons are strongly scattered by solute atoms. Their ability to carry thermal current and heat is significantly reduced, and thus, phonon contribution has larger influence on the overall thermal conductivity [26].

Stress–Strain Measurements

Figure 13 displays the stress–strain ($\sigma - \varepsilon$) curves of SAC155-x Ni alloys subjected to a constant strain rate of $7.82 \times 10^{-4} s^{-1}$ at a measured temperature of 303 ± 1 K. The $\sigma - \varepsilon$ curves of all alloys exhibit a consistent and nearly stable flow stress (σ_{flow}) ranging from 21.3 to 26 MPa at 0.3 strain, forming a plateau-like profile. Notably, the Ni content in the alloys has a significant impact on the shape of

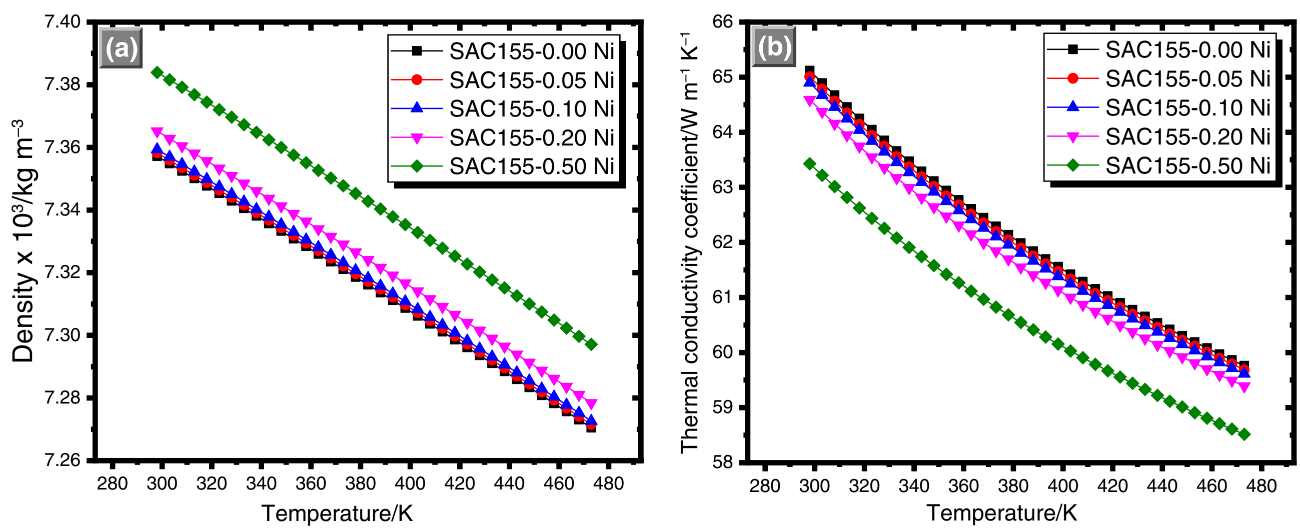

Fig. 12 (**a-b**): **a** Density **b** Thermal conductivity coefficient of (SAC155-x Ni) solder alloys as function in temperature

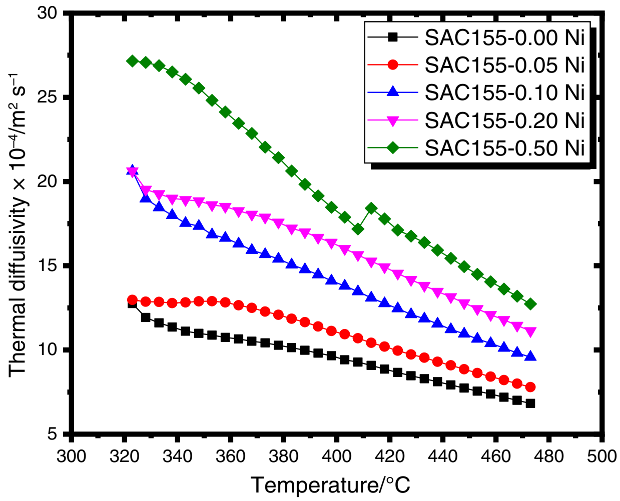

Fig. 13 Thermal diffusivity as function in temperature for (SAC155-x Ni) solder alloys

these curves. Moreover, the stress flow of SAC155-0.5Ni is significantly greater than that of the Ni-free alloy, with an increase of approximately 22.1%. Furthermore, Table 6 summarizes the values of the elasticity tensile modulus (YM), ultimate tensile strength (UTS), and yield stress (YS) for the SAC155-x Ni alloys. The addition of 0.5 mass % Ni exerts a remarkable influence on the tensile parameters. These findings are significant as they indicate a considerable increase in both Young's modulus (YM) and ultimate tensile strength (UTS). YM shows an impressive 55.4% increase, while UTS and YS exhibit a notable improvement of approximately 20.45% and 82.8%, respectively, when compared to the Ni-free solder alloy.

The constant flow stress is a result of the work hardening and dynamic recovery (recrystallization) that occurs during the plastic deformation process [5]. The reason for the enhancement in both flow stress and ultimate tensile stress values in alloys with higher amounts of nickel could be attributed to the integration of intermetallic compounds (IMC) into a β-Sn matrix [8]. So, the volume fraction percent and distribution of the embedding IMCs within the β-Sn matrix help to restrict the movement of dislocations. Then, the mobility of dislocations in the SAC155-0.5Ni alloy is more complex compared to other alloys, resulting in an enhanced increase in flow stress. Moreover, the homogeneous distribution of IMCs within the β-Sn phase contributes to the improvement of the tensile properties [13]. This distribution effectively clears the grain boundary, creating a high potential barrier that impedes dislocation movement. As a result, the addition of Ni enhanced the tensile properties of SAC155 alloy by creating focused dislocation pileups at the boundaries between grains. Therefore, they effectively hindered the growth of grain boundaries and enhanced the friction force, thereby restricting the sliding of the $\beta - Sn$ grains [43].

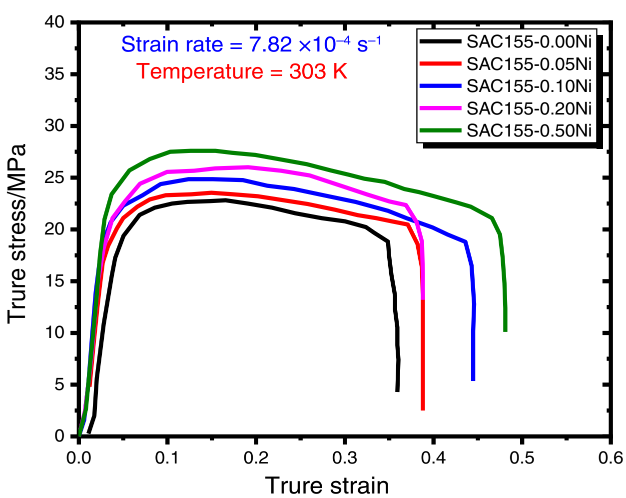

Fig. 14 Stress–Strain graph of SAC155-x Ni solder alloys under strain rate of 7.82×10^{-4} s^{-1} at the temperature 303 K

On the other hand, from Table 6, the comparison of the tensile parameters between Sn-3.5Ag, Sn-Ag-Cu (SAC), Sn-2.0Ag-0.5Cu-0.05Ni (SAC(205)-0.05Ni, and SAC155-x Ni alloys shows that yield stress of SAC155-xNi alloys has a higher yield stress than SAC (205) alloy. This indicates that Ni-containing alloys have a better resistance to plastic deformation and it can withstand a higher maximum load before breaking [44–47]. Also, Young's modulus of SAC155-xNi alloys has a lower Young's modulus than Sn-3.5Ag alloy, which means that it is more elastic and less stiff. This can be beneficial for reducing thermal stress in solder joints [44, 46]. Moreover, ductility or elongation of SAC155-xNi alloys has a lower values than Sn-3.5Ag, which means that it has a lower strain capacity and more brittle and prone to cracking. This can be detrimental for the reliability of solder joints under cyclic loading. In summary, SAC155-xNi alloys have some advantages over Sn-Cu-Ag in terms of yield stress and Young's modulus, but it also has some disadvantages in terms of elongation and ductility [44, 46, 47].

Conclusions

A carefully crafted plan has been implemented to integrate Ni additions ranging from 0.05 to 0.5 mass% to create a refined microstructure in SAC155-x Ni solder alloys. The microstructural outcomes are evident that all SAC155-xNi alloys contain Ag_3Sn, Cu_6Sn_5, and $(Ni, Cu)_6Sn_5$ IMCs. Meanwhile, the SAC155-0.5Ni contains a new IMC named $Cu_8Ni_3Sn_9$ besides the well-known $(Cu, Ni)_3Sn_4$ IMC. Thermodynamic calculations confirmed the presence of these

Table 5 The experimental and calculated values of density, specific heat capacity, thermal diffusivity, and thermal conductivity of the studied SAC155-X Ni alloys in the temperature range 303 –423 K

Physical property	Temperature (K)	SAC155-0.0 Ni		SAC155-0.05Ni		SAC155-0.1Ni		SAC155-0.2 Ni		SAC155-0.5 Ni	
		Cal	Exp	Cal	Exp	Cal	Exp	Cal	Exp	Cal	Exp
Density $\times 10^3$ (kg.m^{-3})	303	7.35484	7.323	7.35587	7.323	7.35699	7.343	7.36281	7.345	7.38156	7.367
	323	7.34533	7.323	7.34636	7.323	7.34748	7.323	7.35330	7.344	7.37204	7.364
	373	7.32107	7.317	7.3210	7.317	7.32322	7.316	7.32903	7.319	7.34775	7.332
	423	7.29612	7.189	7.29715	7.095	7.29827	7.119	7.30407	7.175	7.32277	7.288
Specific Heat $\times 10^3$ (J.kg^{-1}.K$^{-1)}$	303	0.2290	0.3311	0.2291	0.3223	0.2292	0.3132	0.2294	0.2772	0.2303	0.2887
	323	0.2318	0.68372	0.2321	0.67104	0.2322	0.42122	0.2324	0.4191	0.2330	0.3119
	373	0.2398	0.81672	0.2398	0.6918	0.2431	0.54111	0.2411	0.47211	0.2408	0.3119
	423	0.2478	0.96346	0.2476	0.83669	0.2480	0.66805	0.2480	0.5695	0.2486	0.4751
Thermal Diffusivity $\times 10^{-4}$ (m^2.s^{-1})	303	38.5290	25.815	38.441	26.369	38.3543	26.9782	38.1102	30.1932	37.1873	28.6185
	323	12.753	12.447	12.97101	12.608	20.62726	19.8778	20.62039	19.5412	27.15466	26.1335
	373	10.4179	10.083	12.2792	11.891	15.67307	15.1192	17.87285	17.0239	22.03995	24.9067
	423	8.6637	8.372	9.96151	9.7128	12.45729	12.0164	14.54306	13.8448	17.11793	15.8802
Thermal conductivity (W.m^{-1}.K^{-1})	303	64.89301	62.5868	64.78307	62.2364	64.67395	62.0452	64.3693	61.4743	63.21736	60.8674
	323	64.04746	62.3214	63.94319	61.9583	63.83941	61.3150	63.54725	60.1452	62.43778	60.0243
	373	62.29148	60.2562	62.19942	60.1894	62.10717	59.8531	61.84201	58.8240	60.82457	56.958
	423	60.90137	57.9856	60.81952	57.6583	60.73688	57.1482	60.4943	56.5723	59.5541	54.9855

Table 6 Tensile parameters of SAC155-x Ni solder alloys at tested temperature 303 K and strain rate ($\dot{\varepsilon}$) $7.82 \times 10^{-4} s^{-1}$

alloy	Y.M/GPa	YS/MPa	UTS/MPa	Elongation %	Reference
SAC155-0.00 Ni	10.1	11.6	22.93	35.8	This study
SAC155-0.05 Ni	11.2	17.5	23.52	38.7	This study
SAC155-0.10 Ni	11.7	18.8	24.84	44.5	This study
SAC155-0.20 Ni	12.8	193	25.87	38.8	This study
SAC155-0.50 Ni	15.7	21.2	27.62	48.1	This study
SAC (205)-0.05Ni	–	12.6	31.2	74.4	[21]
SAC (205)	–	11.0	30.7	92.8	[21]
SAC (305)	–	–	39.0	55	[21]
Sn-3.5Ag	26.2	22.5	26.7	24	[44]

IMCs. The formation of (Ni, Cu)3Sn4 IMC has been motivated due to their low Gibbs free energy, especially when Ni wt.% is added to a sufficient level. The DSC analysis of alloys disclosed the addition of Ni has increased their melting point from 229.0 to 231.2 ℃ with the low pasty range. The rise of Ni content in the alloys led to lower values of C_p^{max} from 5.54×10^3J.kg^{-1}.K^{-1} to 4.97×10^3J.kg^{-1}.K^{-1}, meanwhile, increasing the energy of arrangement (Q) from 11.36 to 13.41 kJ.mole^{-1}. Obviously, the thermal diffusivity (a) of SAC155-0.5Ni alloys decreases semi-linearly from 27.18×10^{-4} to 12.71×10^{-4}m^2.s^{-1} as the temperature rises from 325 to 473 K, with a reduction of 53.2%. The strength and ductility of the SAC155-0.5Ni alloy are greatly improved, showing a 20.45% and 34.4% increase, respectively. These enhancements in tensile properties of SAC155-xNi alloy are related to dislocation pileups at of $\beta - Sn$ grain boundaries.

Author Contributions EAE contributed to Idea, Conceptualization, Methodology, Writing, Reviewing and Editing, and Supervision; AF contributed to Idea and Supervision; MMM contributed to data collection and graphical design; GS contributed to Idea, Supervision, Methodology, Writing, and Reviewing; and MA contributed to Investigation, Validation, and Writing.

Funding Open access funding provided by The Science, Technology & Innovation Funding Authority (STDF) in cooperation with The Egyptian Knowledge Bank (EKB).

Data Availability No data were used in this research from any other articles.

Declarations

Conflict of Interest The authors declare that they have no known competing financial interests or personal relationships that could have appeared to influence the work reported in this paper.

References

1. Manasijević D, Balanović L, Marković I, Gorgievski M, Stamenković U, Božinović K, et al. Microstructural analysis and thermal conductivity of the Ag–Bi–Sn alloys. Thermochim Acta. 2022;717:179344.
2. Wang H, Zhang K, Zhang M. Fabrication and properties of Ni-modified graphene nanosheets reinforced Sn-Ag-Cu composite solder. J Alloys Compd [Internet]. 2019;781:761–72. https://doi.org/10.1016/j.jallcom.2018.12.080.
3. El-Daly AA, Eid NAM, Ibrahiem AA. Synergic effect of Te, Ni and MWCNT on creep behavior and microstructural evolution of Sn-1.0Ag-0.7Cu low-Ag solder. J Alloys Compd. 2022;902:163808. https://doi.org/10.1016/j.jallcom.2022.163808.
4. Zhang H, Xiao Y, Xu Z, Yang M, Zhang L, Yin L, et al. Effects of Ni-decorated reduced graphene oxide nanosheets on the microstructural evolution and mechanical properties of Sn-3.0Ag-0.5Cu composite solders. Intermetallics. 2022;150:107683. https://doi.org/10.1016/j.intermet.2022.107683.
5. Eid EA, Deghady AM, Fouda AN. Enhanced microstructural, thermal and tensile characteristics of heat treated Sn-5.0Sb-0.3Cu (SSC-503) Pb-free solder alloy under high pressure. Mater Sci Eng A. 2019;743:726–32. https://doi.org/10.1016/j.msea.2018.11.137.
6. El Basaty AB, Deghady AM, Eid EA. Influence of small addition of antimony (Sb) on thermal behavior, microstructural and tensile properties of Sn-9.0Zn-0.5Al Pb-free solder alloy. Mater Sci Eng A. 2017;701:245–53. https://doi.org/10.1016/j.msea.2017.06.092.
7. El-Daly AA, Ibrahiem AA, Eid NAM. Development of Sn-1.0Ag-0.7Cu composite solder with improved resistivity and strength–ductility synergy through additions of Ni, Te and MWCNT. J Mater Sci Mater Electron. 2021;32:19871–89. https://doi.org/10.1007/s10854-021-06512-2.
8. Che FX, Zhu WH, Poh ESW, Zhang XR, Zhang X, Chai TC, et al. Creep properties of Sn-1.0Ag-0.5Cu lead-free solder with Ni addition. J Electron Mater. 2011;40:344–54.
9. Zhao X, Saka M, Yamashita M, Hokazono H. The effect of adding Ni and Ge microelements on the electromigration

resistance of low-Ag based SnAgCu solder. Microsyst Technol. 2012;18:2077–84.
10. Attia Negm SE, Moghny ASA, Ahmad SI. Investigation of thermal and mechanical properties of Sn-Zn and Sn-Zn-Bi near-eutectic solder alloys. Results Mater. 2022;15:100316. https://doi.org/10.1016/j.rinma.2022.100316.
11. Deghady AM, Fadel MM, Eid EA. The doping of SZC solders with bismuth to improve their thermal and tensile characteristics for microelectronic applications. J Mater Sci Mater Electron. 2022;33:4831–46. https://doi.org/10.1007/s10854-021-07672-x.
12. Fouda AN, Eid EA. Role of graphene oxide (GO) for enhancing the solidification rate and mechanical properties of Sn–6.5Zn–0.4 mass% Cu Pb-free solder alloy. J Mater Sci Mater Electron. 2022;33:522–40. https://doi.org/10.1007/s10854-021-07324-0.
13. Eid EA, El-Khawas EH, Abd-Elrahman AS. Impact of Sb additives on solidification performance, microstructure enhancement and tensile characteristics of Sn-6.5Zn-0.3Cu Pb-free solder alloy. J Mater Sci Mater Electron. 2019;30:6507–18. https://doi.org/10.1007/s10854-019-00956-3.
14. Zhou D, Haseeb ASMA, Andriyana A. Mechanical performance of advanced multicomponent lead-free solder alloy under thermal aging. Mater Today Commun. 2022;33:104430. https://doi.org/10.1016/j.mtcomm.2022.104430.
15. Du Y, Wang Y, Ji X, Jia Q, Zhang F, Guo F. Impact of Ni-coated carbon fiber on the interfacial (Cu, Ni)6Sn5 growth of Sn-3.5Ag composite solder on Cu substrate during reflow and isothermal aging. Mater Today Commun. 2022;31:103572. https://doi.org/10.1016/j.mtcomm.2022.103572.
16. Dariavach N, Callahan P, Liang J, Fournelle R. Intermetallic growth kinetics for Sn-Ag, Sn-Cu, and Sn-Ag-Cu lead-free solders on Cu, Ni, and Fe-42Ni substrates. J Electron Mater. 2006;35:1581–92.
17. Ramli MII, Salleh MAAM, Abdullah MMAB, Zaimi NSM, Sandu AV, Vizureanu P, et al. Formation and growth of intermetallic compounds in lead-free solder joints: a review. Materials (Basel). 2022;15:1–21.
18. Karunaratne MSA, Kyaw S, Jones A, Morrell R, Thomson RC. Modelling the coefficient of thermal expansion in Ni-based superalloys and bond coatings. J Mater Sci. 2016;51:4213–26.
19. Oliveira R, Cruz C, Barros A, Bertelli F, Spinelli JE, Garcia A, et al. Thermal conductance at Sn-0.5mass%Al solder alloy/substrate interface as a factor for tailoring cellular/dendritic growth. J Therm Anal Calorim. 2022;147:4945–58. https://doi.org/10.1007/s10973-021-10755-w.
20. Silva LS, Souza JS, Silva RAG. Effects of Ag addition on phase transitions, microstructures and solder/copper interfaces of Sn 99.1–x Cu 0.9 Ag x alloys. J Therm Anal Calorim. 2019;136:2205–10. https://doi.org/10.1007/s10973-018-7893-4.
21. El-Daly AA, El-Taher AM. Improved strength of Ni and Zn-doped Sn-2.0Ag-0.5Cu lead-free solder alloys under controlled processing parameters. Mater Des. 2013;47:607–14. https://doi.org/10.1016/j.matdes.2012.12.081.
22. El-Daly AA, El-Taher AM, Dalloul TR. Improved creep resistance and thermal behavior of Ni-doped Sn-3.0Ag-0.5Cu lead-free solder. J Alloys Compd. 2014;587:32–9. https://doi.org/10.1016/j.jallcom.2013.10.148.
23. Zribi A, Chromik RR, Presthus R, Teed K, Zavalij L, DeVita J, et al. Solder metallization interdiffusion in microelectronic interconnects. IEEE Trans Components Packag Technol. 2000;23:383–7.
24. Chen HM, Wang Q, Geng DL, Wang HP. Specific heat, thermal diffusivity, and thermal conductivity of Ag–Si alloys within a wide temperature range of 293–823 K. J Phys Chem Solids. 2021;153:109997. https://doi.org/10.1016/j.jpcs.2021.109997.
25. Parker WJ, Jenkins RJ, Butler CP, Abbott GL. Flash method of determining thermal diffusivity, heat capacity, and thermal conductivity. J Appl Phys. 1961;32:1679–84.
26. Manasijević D, Balanović L, Marković I, Gorgievski M, Stamenković U, Đorđević A, et al. Structural and thermal properties of Sn–Ag alloys. Solid State Sci. 2021;119:106685.
27. Gaal PS, Thermitus MA, Stroe DE. Thermal conductivity measurements using the flash method. J Therm Anal Calorim. 2004;78:185–9.
28. El-Daly AA, Hammad AE, Fawzy A, Nasrallh DA. Microstructure, mechanical properties, and deformation behavior of Sn-1.0Ag-0.5Cu solder after Ni and Sb additions. Mater Des. 2013;43:40–9. https://doi.org/10.1016/j.matdes.2012.06.058.
29. Chantaramanee S, Sungkhaphaitoon P. Investigation of microstructure, thermal properties, and mechanical performances of Ni-added Sn-5.0Sb-0.5Cu/Cu solder joints. Microelectron Reliab. 2021;127:114421. https://doi.org/10.1016/j.microrel.2021.114421.
30. Hammad AE. Enhancing the ductility and mechanical behavior of Sn-1.0Ag-0.5Cu lead-free solder by adding trace amount of elements Ni and Sb. Microelectron Reliab. 2018;87:133–41. https://doi.org/10.1016/j.microrel.2018.06.015.
31. Xin M, Wang X, Sun F. Microstructure evolution, IMC growth, and microhardness of Cu, Ni, Ag-microalloyed Sn–5Sb/Cu solder joints under isothermal aging. J Mater Sci Mater Electron. 2022;33:25025–40. https://doi.org/10.1007/s10854-022-09210-9.
32. Hu X, Xu T, Jiang X, Li Y. Interfacial reaction and IMCs growth behavior of Sn3Ag0.5Cu/Ni solder bump during aging at various temperatures. J Mater Sci Mater Electron. 2016;27:4245–52.
33. Gao F, Qu J. Elastic moduli of (Ni, Cu) 3Sn 4 ternary alloys from first-principles calculations. J Electron Mater. 2010;39:2429–34.
34. Gao H, Wei F, Sui Y, Qi J, He Y, Meng Q. Effect of nickel (Ni) on the growth rate of Cu 6 Sn 5 intermetallic compounds between Sn–Cu–Bi solder and Cu substrate. J Mater Sci Mater Electron. 2019;30:2186–91. https://doi.org/10.1007/s10854-018-0490-2.
35. Liu XJ, Wang CP, Gao F, Ohnuma I, Ishida K. Thermodynamic calculation of phase equilibria in the Sn-Ag-Cu-Ni-Au system. J Electron Mater. 2007;36:1429–41.
36. Lin CY. Interfacial reaction between Ni particle reinforcements and liquid Sn-based eutectic solders. Solder Surf Mt Technol. 2021;33:240–5.
37. Sun Q, Wang J, Wang XN, Zhou XW, Tang XX, Akira K. Cu aggregation behavior on interfacial reaction of Sn-3.0Ag-0.5Cu/ENIG solder joints. Mater Lett. 2023;348:134659. https://doi.org/10.1016/j.matlet.2023.134659.
38. Guo Z, Saunders N, Miodownik P, Schillé JP. Modeling material properties of lead-free solder alloys. J Electron Mater. 2008;37:23–31.
39. Saunders N, Guo Z, Li X, Miodownik AP, Schillé JP. Using JMatPro to model materials properties and behavior. Jom. 2003;55:60–5.
40. El-Taher AM, Mansour SA, Lotfy IH. Robust effects of In, Fe, and Co additions on microstructures, thermal, and mechanical properties of hypoeutectic Sn–Zn-based lead-free solder alloy. J Mater Sci Mater Electron. 2023;34:1–20. https://doi.org/10.1007/s10854-023-09969-5.

41. Gumaan MS, Shalaby RM, Ali EAM, Kamal M. Copper effects in mechanical, thermal and electrical properties of rapidly solidified eutectic Sn–Ag alloy. J Mater Sci Mater Electron. 2018;29:8886–94. https://doi.org/10.1007/s10854-018-8906-6.
42. Morando C, Fornaro O, Garbellini O, Palacio H. Thermal properties of Sn-based solder alloys. J Mater Sci Mater Electron. 2014;25:3440–7.
43. Sayyadi R, Khodabakhshi F, Javid NS, Khatibi G. Influence of graphene content and nickel decoration on the microstructural and mechanical characteristics of the Cu/Sn–Ag–Cu/Cu soldered joint. J Mater Res Technol. 2020;9:8953–70. https://doi.org/10.1016/j.jmrt.2020.06.026.
44. Ren W, Qian Z, Liu S. Scale effect on packaging materials. Proc - Electron Components Technol Conf. 1999;1229–34.
45. Kong YG, Kong ZG, Shi FM. Microstructure and mechanical property of Sn–Ag–Cu solder material. Rare Met. 2017;36:193–7.
46. Kim KS, Huh SH, Suganuma K. Effects of fourth alloying additive on microstructures and tensile properties of Sn-Ag-Cu alloy and joints with Cu. Microelectron Reliab. 2003;43:259–67.
47. Yakymovych A, Švec P, Orovcik L, Bajana O, Ipser H. Nanocomposite SAC Solders: the effect of adding Ni and Ni-Sn nanoparticles on morphology and mechanical properties of Sn-3.0Ag-0.5Cu solders. J Electron Mater. 2018;47:117–23.

Publisher's Note Springer Nature remains neutral with regard to jurisdictional claims in published maps and institutional affiliations.